

HIGH-VELOCITY BIPOLAR MOLECULAR EMISSION FROM AN AGN TORUS

JACK F. GALLIMORE¹, MOSHE ELITZUR^{2,3}, ROBERTO MAIOLINO^{4,5}, ALESSANDRO MARCONI^{6,7}, CHRISTOPHER P. O'DEA⁸,
DIETER LUTZ⁹, STEFI A. BAUM⁸, ROBERT NIKUTTA¹⁰, C. M. V. IMPELLIZZERI¹¹, RICHARD DAVIES⁹, AMY E. KIMBALL¹²,
AND ELEONORA SANI¹³

¹Dept. of Physics & Astronomy, Bucknell University, Lewisburg, PA 17837; jgallimo@bucknell.edu

²Astronomy Dept., University of California, Berkeley, CA 94720

³Physics & Astronomy, University of Kentucky, Lexington, KY 40506

⁴Cavendish Laboratory, University of Cambridge, 19 J. J. Thomson Ave, Cambridge CB3 0HE, UK

⁵Kavli Institute for Cosmology, University of Cambridge, Madingley Road, Cambridge CB3 0HA, UK

⁶Dipartimento di Fisica e Astronomia, Università di Firenze, via G. Sansone 1, 50019, Sesto Fiorentino (Firenze), Italy

⁷INAF-Osservatorio Astrofisico di Arcetri, Largo E. Fermi 5, 50125, Firenze, Italy

⁸University of Manitoba, Department of Physics and Astronomy, Winnipeg, MB R3T 2N2, Canada

⁹Max Planck Institute for Extraterrestrial Physics, Giessenbachstrasse 1, D-85748 Garching, Germany

¹⁰Instituto de Astrofísica, Facultad de Física, Pontificia Universidad Católica de Chile, 306, Santiago 22, Chile

¹¹Joint ALMA Office, Alonso de Cordova 3107, Vitacura, Santiago, Chile

¹²National Radio Astronomy Observatory, 1003 Lopezville Rd., Socorro, NM 87801, USA

¹³European Southern Observatory, Alonso de Cordova 3107, Vitacura, Santiago, Chile

ABSTRACT

We have detected in ALMA observations CO $J = 6 \rightarrow 5$ emission from the nucleus of the Seyfert galaxy NGC 1068. The low-velocity (up to ± 70 km s⁻¹ relative to systemic) CO emission resolves into a 12×7 pc structure, roughly aligned with the nuclear radio source. Higher-velocity emission (up to ± 400 km s⁻¹) is consistent with a bipolar outflow in a direction nearly perpendicular ($\simeq 80^\circ$) to the nuclear disk. The position-velocity diagram shows that in addition to the outflow, the velocity field may also contain rotation about the disk axis. These observations provide compelling evidence in support of the disk-wind scenario for the AGN obscuring torus.

Keywords: galaxies: active — galaxies: nuclei — galaxies: Seyfert — galaxies: individual (NGC 1068)
— quasars: general

1. INTRODUCTION

The great diversity of AGN classes has been explained by a single unified scheme. The nuclear activity is powered by accretion onto a supermassive ($\sim 10^6$ – $10^{10} M_\odot$) black hole. The active region is surrounded by an obscuring, dusty toroidal structure so that sources viewed face-on are recognized as type 1 AGN, and those observed edge-on are type 2 (e.g., Antonucci 1993; Urry & Padovani 1995). However, the origin and nature of the obscuring torus remain far from understood, with proposed models broadly divided into two main classes. In one, the torus is a stationary doughnut-like structure (Krolik & Begelman 1988), and its large dimensions ($\gtrsim 100$ pc) place it well outside the black hole (BH) radius of gravitational influence (Pier & Krolik 1993; Granato & Danese 1994). In the other, a dynamic picture is employed: the torus is made of gas processed by the accretion disk and expelled outwards in a disk wind; the outflow inner part is atomic and ionized, giving rise to

broad line emission, its outer regions are molecular and dusty, resulting in a compact (well within the BH gravitational potential), axisymmetric obscuring structure that mimics a hydrostatic toroidal distribution (Elitzur & Shlosman 2006, and references therein).

Beginning with the VLTI detection of the nucleus in NGC 1068 (Jaffe et al. 2004), infrared (IR) observations have established the compact dimensions of AGN dusty tori (Elitzur 2008; Nenkova et al. 2008). Optical–near-IR reverberation lags in Type 1 Seyferts are consistent with sub-parsec torus inner radii (e.g., Vazquez et al. 2015, and references therein). Further confirmation comes from recent ALMA observations by García-Burillo et al. (2016; GB16 hereafter). They detected molecular emission from the NGC 1068 torus, contained within ~ 3 pc from the center. However, although the torus’s compact dimensions are now firmly established, its kinematics and dynamic origin remain uncertain. Water maser observations provide support for the disk-

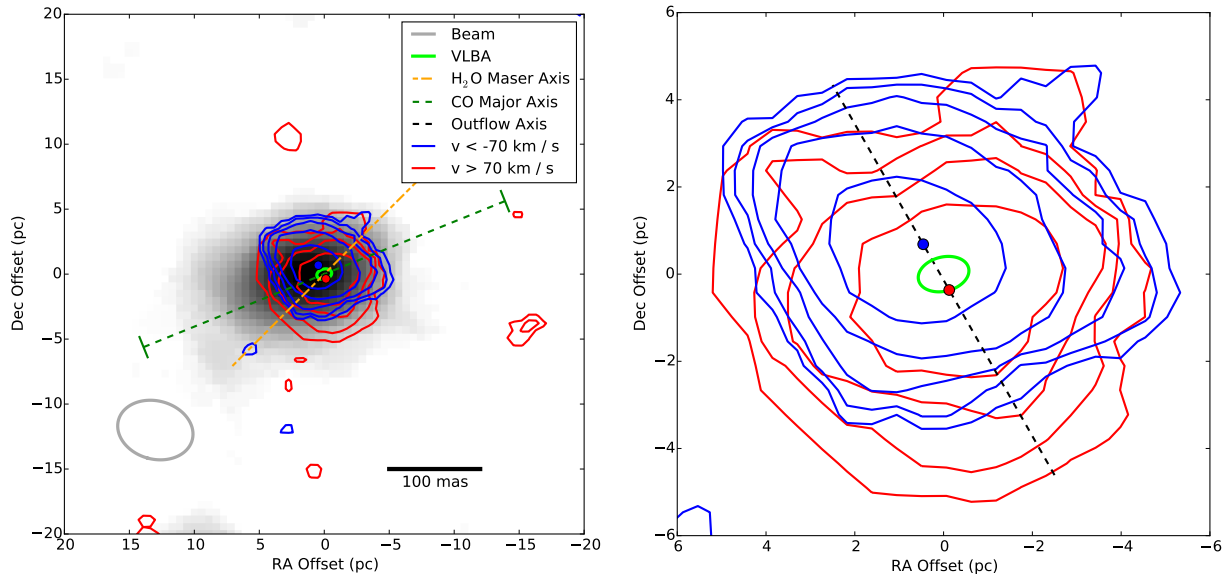


Figure 1. *Left:* CO image integrated between radial velocities -70 and $+70$ km s^{-1} relative to systemic, shown as grayscale linearly stretched between 0.30 and 7.0 $\text{Jy km s}^{-1} \text{beam}^{-1}$. Position offsets are presented in physical units and are measured with respect to the centroid of the 5 GHz VLBA image of S1, the nuclear plasma disk whose orientation and location are illustrated by the green ellipse. The 100 mas scale bar in the lower right corner indicates the angular scale. The dashed green line (PA 112°) illustrates the CO image major axis and the extraction axis for the position-velocity diagram (see text for details). The end-caps on the major axis line show the three-pixel (24 mas, or 1.8 pc) extraction width for the position-velocity diagram. Red and blue contours trace the integrated CO emission over velocities $> +70$ km s^{-1} and < -70 km s^{-1} , respectively. The contour levels are 0.30 , 0.50 , 0.83 , 1.4 , and 2.3 $\text{Jy km s}^{-1} \text{beam}^{-1}$. The alternating dashed orange line (PA 135°) shows the orientation of the H_2O maser disk, stretched beyond its ~ 1.7 pc major axis to emphasize its orientation at the scale of the plot. *Right:* Zoom-in on the high-velocity contours; the contour peaks are marked by colored dots. The red and blue contours are systematically displaced from each other, with their peaks separated by 1.2 pc along the axis PA 33° , which is traced by the dashed black line. This displacement is indicative of a bipolar outflow roughly orthogonal to the nuclear disk.

wind scenario in Circinus (Greenhill et al. 2003) and NGC 3079 (Kondratko et al. 2005) but the tight constraints on strong maser emission do not allow a complete sampling of the molecular gas.

Here we report our own ALMA observations of thermal CO emission from the NGC 1068 torus. We adopt a distance to the source of 14.4 Mpc (Bland-Hawthorn et al. 1997). The scale is $1'' = 70$ pc.

2. OBSERVATIONS AND DATA PROCESSING

We observed NGC 1068 in Band 9 ($\lambda \sim 450 \mu\text{m}$) during ALMA Cycle 2 (project code 2013.1.00014.S). Total time on source was 32.1 minutes. The baseline range was 15 – 1466 m, and the synthetic restoring beam (angular resolution) is $0''.084 \times 0''.064$, PA 75° , or 5.9×4.5 pc. Resulting images are insensitive to structures larger than about 270 pc ($3.8''$). Source observations were interleaved with short scans of the nearby bright calibrator source J0217+0144, located 6.5° from NGC 1068. Spectral windows were tuned to observe three independent continuum bands, 2 GHz bandwidth each, and one line window for CO ($J = 6 \rightarrow 5$; $\nu_0 = 691.47308$ GHz; hereafter, CO) in ~ 0.21 km s^{-1} channels spanning $\sim \pm 400$ km s^{-1} total bandwidth. Calibration and data reduction followed standard procedures for ALMA obser-

vations in CASA (CASA v.4.3.1; McMullin et al. 2007). NGC 1068 proved bright enough for self-calibration over scan intervals. Two rounds of phase-only self-calibration reduced sidelobe artifacts and improved the background rms.

The photometric accuracy, $\sim 10\%$, is limited by the photometric uncertainties of the flux calibrators (3C454.3 and J2253+1608). The absolute astrometric accuracy of these ALMA observations are limited by the transfer of calibration solutions from the complex gain calibrators to NGC 1068. We estimate that the final absolute astrometric accuracy¹ of our observations is 1.3 pc (19 mas). This systematic uncertainty is large compared to the ~ 4 pc scale of the nuclear environment. We therefore adopted an astrometric correction by aligning the Band 9 continuum peak to the position of the active nucleus (cf. GB16). In angular units, the shift moves the Band 9 continuum peak 9.5 mas west and 11 mas south. In physical units, the shift is 1.0 pc, which lies within the 1.3 pc systematic uncertainty.

Images and data cubes were produced using Briggs weighting (Briggs 1995) and multiscale CLEAN decon-

¹ Based on information provided by the ALMA Helpdesk.

olution (Cornwell 2008). The CO spectral line cube was binned to 10 km s^{-1} channel-widths during imaging and deconvolution. The background rms noise levels are $0.49 \text{ mJy beam}^{-1}$ and $5.3 \text{ mJy beam}^{-1}$ for Band 9 continuum and the CO channel maps, respectively.

3. RESULTS

GB16 performed similar observations of NGC 1068, and their continuum and integrated line maps resemble ours. Like GB16, we detect continuum and molecular emission located at the position of the nuclear radio source, S1, and its associated H_2O vapor maser disk (Greenhill & Gwinn 1997; Gallimore et al. 2004). The detected CO spans the full $\pm 400 \text{ km s}^{-1}$ spectral range. Figure 1 shows the CO image of S1 integrated over three bins: blueshifted, $v < -70 \text{ km s}^{-1}$ (blue contours); systemic, $-70 \leq v \leq +70 \text{ km s}^{-1}$ (greyscale); and redshifted, $v > +70 \text{ km s}^{-1}$ (red contours), where v is the observed radial velocity relative to systemic. The choice of $\pm 70 \text{ km s}^{-1}$ for velocity bin edges was based on initial inspection of the data and the analysis of near-infrared H_2 emission (Galliano & Alloin 2002; Müller Sánchez et al. 2009). At low v , the source resolves along PA 112° (green dashed line), extending $\sim 10 \text{ pc}$ southeast of the VLBA source.

The CO source is unresolved in the integrated blueshifted and redshifted velocity bins. However, the blue contours are systematically displaced with respect to the red ones along the dashed black axis in Figure 1; in particular, the position of the blueshifted velocity peak is displaced 1.2 pc northeast (PA $\simeq 33^\circ$) of the redshifted peak. The displacement axis is roughly orthogonal ($78^\circ \pm 2^\circ$) to the line of masers, which trace a nearly edge-on disk. Thus *the high-velocity CO emission is consistent with a bipolar outflow along the AGN axis*, similar to the outflow inferred from observations of ionized gas in the narrow line region of the NGC 1068 nucleus (Crenshaw & Kraemer 2000).

Additional evidence for the CO bipolar outflow comes from the spectral map in the left panel of Figure 2. Here we show the locations of CO emission peaks from the full spectral line cube. We performed spectroastrometry using `find_peaks` from the `photutils` package of `Astropy` (Astropy Collaboration et al. 2013). Peaks $> 3.0\sigma$ on individual channel maps were recorded, and their positions were refined using a local 2-D Gaussian fit. The map shows that each high-velocity bin predominates in one of the two hemispheres defined by the maser disk, as expected from a bipolar outflow roughly aligned with the inner part of the radio jet, whose contours are also shown. We propose that the CO emission arises from a bipolar outflow around the axis of the AGN accretion disk. Molecular gas moving in the plane of the sky contributes to the systemic-velocity bin, whereas gas on the

near (far) side of the plane appears in the blue (red) bin.

The outflow axis of ionized gas traced by optical emission lines in the narrow-line region is inclined 5° out of the plane of the sky (Crenshaw & Kraemer 2000), and we assume the same for the CO outflow. Can such a small inclination produce the red-blue spatial separation observed in CO? To test this possibility we conducted a numerical simulation of a bipolar outflow. We employ a truncated cone geometry with a disk base diameter of 1 pc (comparable to the H_2O maser disk), 4.4 pc total bicone height (based on the spread of CO features in Figure 2), and half-opening angle of 30° . To model the outflow, we randomly placed a total of 10^4 clumps inside the cone. Clumps were evenly distributed in cylindrical radius ρ (i.e., radius projected onto the disk plane) and distance along the polar axis. The direction of motion for a clump is vertical for clumps directly above and below the disk (i.e., clumps with $\rho \leq 0.5 \text{ pc}$) and radial from the edge of the disk for clumps with $\rho > 0.5 \text{ pc}$. We further assume uniform acceleration from 30 km s^{-1} at the molecular disk to 800 km s^{-1} at the cone height; these values were selected from interactive trials to give a reasonable match to the observations. Finally, all clumps are equally luminous point sources of CO emission, added as beam-shaped, two-dimensional Gaussians to the planes of a simulated data cube. The cone was then inclined by 5° , and we repeated the cube analyses on the simulated data. To simulate the effects of measurement uncertainty, each measured peak position was displaced randomly, assuming 0.5 pc errors, comparable to the relative, observed position uncertainties. The simulation results shown in the right panel of Figure 2 broadly reproduce a parsec-scale asymmetry of redshifted and blueshifted peaks similar to that observed (left panel). This simple simulation was not meant to replicate any physical model or explain every aspect of the data; in particular, the systemic-velocity emission is concentrated to the east, at odds with the random distribution we use. Our simulation is only meant to demonstrate that the small 5° tilt detected in narrow line observations is sufficient to produce the red-blue asymmetry of the excited CO emission.

In addition to the outflow component described above, we also find evidence for rotation consistent with the compact H_2O maser disk. Figure 3 shows the position-velocity (p - v) diagram constructed by slicing the CO spectral line cube along the axis tracing the extended systemic emission. Surface brightnesses were averaged within the 3-pixel extraction width (green dashed lines in Figure 1). The data were smoothed using a Savitzky-Golay filter (7 channels, polynomial order 3; Savitzky & Golay 1964) along the velocity axis for display purposes. The diagram reveals CO emission at very high velocities, with significant ($> 3\sigma$) detections approach-

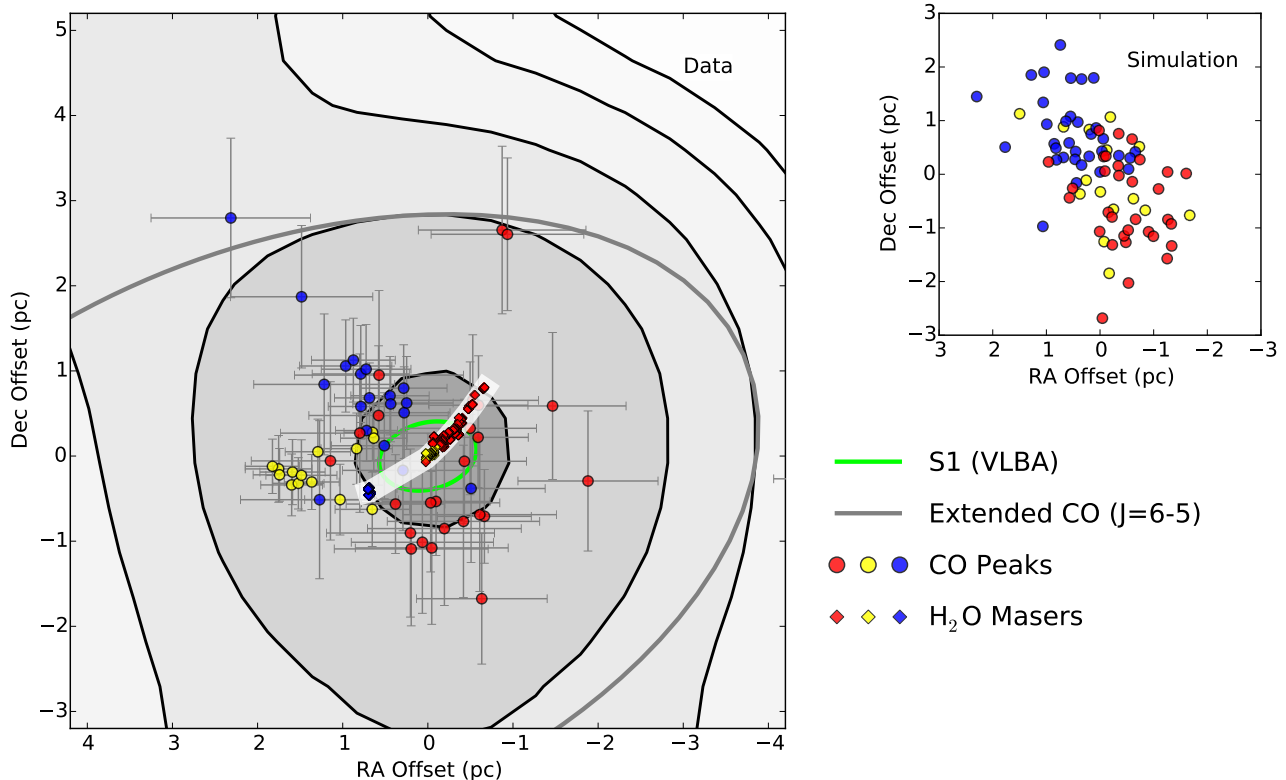


Figure 2. *Left:* The locations of CO emission peaks, marked by colored circles. The colors are coded by radial velocity bins relative to systemic: $v > 70 \text{ km s}^{-1}$ (red), $-70 \leq v \leq 70 \text{ km s}^{-1}$ (yellow), and $v < -70 \text{ km s}^{-1}$ (blue). Following the same velocity color coding, the positions of H₂O maser spots (Greenhill & Gwinn 1997) are plotted as diamonds within the central, white arcuate band. The location and scale of the VLBA radio continuum source is indicated by the green ellipse. The outer gray ellipse illustrates the orientation of the resolved, low velocity CO emission (see Fig. 1). Grayscale contours are from MERLIN 5 GHz observations of the radio jet (Gallimore et al. 2004); the MERLIN beam is 4.2 pc FWHM. *Upper Right:* Spectral map from a simulation of a bipolar outflow with axis tilted 5° from the plane of the sky and rotated to PA 33° (see text for details). Colors are as for the left panel.

ing $v = \pm 400 \text{ km s}^{-1}$ relative to systemic. Also shown are the H₂O maser spots, appearing as a nearly vertical chain centered on the origin. Such a straight line in the p - v diagram is the hallmark of a rotating ring whose angular velocity is the line slope (e.g., Pestalozzi et al. 2009). The fact that the maser line is so straight and narrow implies that all maser spots are located within a radially thin annulus at the disk inner radius. The ALMA data show a similar elongated structure aligned with the maser chain, only covering a wider spread of positions. This component can be interpreted as CO emission from a wider range of rotating regions close to the disk innermost boundary. The thermal CO emission traces these molecular regions more fully than the masers, because strong maser emission is not produced without the fulfilment of some strict constraints on the physical parameters. For example, these constraints likely explain the dearth of blue-shifted maser spots. Additionally, the CO data also show another elongated component, this one closer to the horizontal axis. Its smaller slope implies a lower angular velocity, which in

turn implies a larger radius and can be interpreted as emission from the outer regions of the CO distribution.

An elongated structure in the p - v diagram could also be produced by a collimated jet, in which case the slope is directly related to the jet inclination from the line of sight (Pestalozzi et al. 2009). The existence of two such features with different slopes and the overlap of one of them with the maser line make a jet-based explanation unlikely, indicating that the CO velocity field contains a kinematic component consistent with rotation.

To explore this possibility we simulated the p - v diagram of an edge-on disk with kinematics based on Keplerian rotation around a $1.5 \times 10^7 M_\odot$ central mass that best fits the H₂O maser disk observations (Lodato & Bertin 2003) but with line of nodes rotated 23° to match the p - v slice orientation. To highlight the expected contribution of such a disk, its emissivity was scaled proportional to r^{-2} , where r is the disk radial coordinate. The simulated data were beam-smoothed and binned into 10 km s^{-1} channels to compare with the ALMA observations. The result is shown as transparent, violet-

ence Foundation operated under cooperative agreement by Associated Universities, Inc. This research made use of Astropy, a community-developed core Python package for Astronomy ([Astropy Collaboration et al. 2013](#)). RN acknowledges support by FONDECYT grant No.

3140436. RM acknowledges support from the UK Science and Technology Facilities Council (STFC).

Facility: ALMA

Software: CASA, astropy

REFERENCES

- Antonucci, R. 1993, *ARA&A*, 31, 473
- Astropy Collaboration, Robitaille, T. P., Tollerud, E. J., et al. 2013, *A&A*, 558, A33
- Bland-Hawthorn, J., Gallimore, J. F., Tacconi, L. J., et al. 1997, *Ap&SS*, 248, 9
- Blandford, R. D., & Payne, D. G. 1982, *MNRAS*, 199, 883
- Briggs, D. S. 1995, PhD thesis, The New Mexico Institute of Mining and Technology
- Cornwell, T. J. 2008, *IEEE Journal of Selected Topics in Signal Processing*, 2, 793
- Crenshaw, D. M., & Kraemer, S. B. 2000, *ApJL*, 532, L101
- Elitzur, M. 2008, *New Astronomy Review*, 52, 274
- Elitzur, M., & Ho, L. C. 2009, *ApJL*, 701, L91
- Elitzur, M., & Shlosman, I. 2006, *ApJL*, 648, L101
- Emmering, R. T., Blandford, R. D., & Shlosman, I. 1992, *ApJ*, 385, 460
- Galliano, E., & Alloin, D. 2002, *A&A*, 393, 43
- Gallimore, J. F., Baum, S. A., & O’Dea, C. P. 2004, *ApJ*, 613, 794
- García-Burillo, S., Combes, F., Ramos Almeida, C. and, U. A., et al. 2016, *ApJL*, 823, L12
- Granato, G. L., & Danese, L. 1994, *MNRAS*, 268, 235
- Greenhill, L. J., & Gwinn, C. R. 1997, *Ap&SS*, 248, 261
- Greenhill, L. J., Booth, R. S., Ellingsen, S. P., et al. 2003, *ApJ*, 590, 162
- Jaffe, W., Meisenheimer, K., Röttgering, H. J. A., et al. 2004, *Nature*, 429, 47
- Kartje, J. F., Königl, A., & Elitzur, M. 1999, *ApJ*, 513, 180
- Kondratko, P. T., Greenhill, L. J., & Moran, J. M. 2005, *ApJ*, 618, 618
- Krolik, J. H., & Begelman, M. C. 1988, *ApJ*, 329, 702
- Lodato, G., & Bertin, G. 2003, *A&A*, 398, 517
- McMullin, J. P., Waters, B., Schiebel, D., Young, W., & Golap, K. 2007, in *Astronomical Society of the Pacific Conference Series*, Vol. 376, *Astronomical Data Analysis Software and Systems XVI*, ed. R. A. Shaw, F. Hill, & D. J. Bell, 127
- Müller Sánchez, F., Davies, R. I., Genzel, R., et al. 2009, *ApJ*, 691, 749
- Nenkova, M., Sirocky, M. M., Nikutta, R., Ivezić, Ž., & Elitzur, M. 2008, *ApJ*, 685, 160
- Pestalozzi, M. R., Elitzur, M., & Conway, J. E. 2009, *A&A*, 501, 999
- Pier, E. A., & Krolik, J. H. 1993, *ApJ*, 418, 673
- Savitzky, A., & Golay, M. J. E. 1964, *Analytical Chemistry*, 38, 1627
- Urry, C. M., & Padovani, P. 1995, *PASP*, 107, 803
- Vazquez, B., Galianni, P., Richmond, M., et al. 2015, *ApJ*, 801, 127